

Substituent Effect on Supercapacitive Performances of Conducting Polymer-Based Redox Electrodes: Poly(3',4'-bis(alkyloxy) 2,2':5',2''-terthiophene) Derivatives

Deniz Yiğit , Melis Aykan, Mustafa Güllü

Department of Chemistry, Ankara University, Besevler 06100, Ankara, Turkey

Correspondence to: D. Yiğit (E-mail: dyigit@science.ankara.edu.tr) or M. Güllü (E-mail: gullu@ankara.edu.tr)

Received 23 October 2017; accepted 29 November 2017; published online 00 Month 2017

DOI: 10.1002/pola.28927

ABSTRACT: This work reports the synthesis of novel poly(3',4'-bis(alkyloxy)terthiophene) derivatives (PTTOBu, PTTOHex, and PTTOOct) and their supercapacitor applications as redox-active electrodes. The terthiophene-based conducting polymers have been derivatized with different alkyl pendant groups (butyl-, hexyl-, and octyl-) to explore the effect of alkyl chain length on the surface morphologies and pseudocapacitive properties. The electrochemical performance tests have revealed that the length of alkyl substituent created a remarkable impact over the surface morphologies and charge storage properties of polymer electrodes. PTTOBu, PTTOHex, and PTTOOct-based electrodes have reached up to specific capacitances of 94.3,

227.3, and 443 F g⁻¹ at 2.5 mA cm⁻² constant current density, respectively, in a three-electrode configuration. Besides, these redox-active electrodes have delivered satisfactory energy densities of 13.5, 29.3, and 60.7 W h kg⁻¹ and power densities of 0.98, 1, and 1.1 kW kg⁻¹ with good capacitance retentions after 10,000 charge/discharge cycles in symmetric solid-state micro-supercapacitor devices. © 2017 Wiley Periodicals, Inc. *J. Polym. Sci., Part A: Polym. Chem.* **2017**, *00*, 000–000

KEYWORDS: conducting materials; energy storage; materials science; polymers; redox-active electrodes; solid-state devices; supercapacitors; terthiophenes

INTRODUCTION Over the past 10 years, there has been a ever-increasing demand for innovative electrical energy storage solutions to fulfill the requirements of advance electronic applications. Especially, the fast advancement of portable and flexible consumer electronic products such as roll-up displays, electronic papers, wearable sensors, smart phones, and touch screens makes it necessary to develop low-cost, lightweight, thin and flexible energy storage systems. In this context, supercapacitors, also commonly known as electrochemical capacitors or ultracapacitors, are considered as new generation energy storage devices in terms of their energy and power densities.^{1–3}

Compared to primary and secondary batteries, even though supercapacitors generally deliver lower energy density they have desirable advantages including long cycle lives, high charge capabilities, short charging/discharging times, cost-effective fabrication, and good operational safety.^{4–6} The capacitive performance of a supercapacitor is directly related to the electroactive materials. In particular, morphological and electrochemical features like surface area and porosity, thickness, electrical conductivity, and internal resistance play critical role on charge storage capacity of electrode material.⁷

Therefore, the great majority of recent efforts have been devoted to designing ideal electrode materials possessing high capacitance, high energy density, high power density, and high cycling durability.

In electrochemical double-layer capacitors (EDLCs), carbon-based materials such as carbon nanotubes,^{8,9} graphenes,^{10,11} carbon nanofibers,¹² and aerogels¹³ have been widely used as electrode materials because of their outstanding electronic properties and excellent mechanical stabilities. These carbonaceous materials use a non-Faradaic mechanism based on physical sorption/desorption to store charges and release energy, so do conventional dielectric capacitors.¹⁴ Hence, EDLCs usually provide low capacitance and energy density despite the fact that they have high surface area, highly porous network, fast ion kinetic, good chemical and thermal stability, and excellent mechanical strength.¹⁵

Transition metal oxides (MOx) and π -conjugated conducting polymers are promising electrode material groups for electrochemical energy storage applications.^{16–21} In contradistinction to carbon-based structures, MOx- or conducting polymer-based electrode materials store charge through not

Additional Supporting Information may be found in the online version of this article.

© 2017 Wiley Periodicals, Inc.

only electrostatic ion sorption/desorption mechanism, but also a fast and reversible Faradaic redox processes which results in much higher specific capacitance and power density values than EDLCs.^{22,23} To date, various MOx with variable valence states, TiO₂,²⁴ MnO₂,²⁵ SnO₂,²⁶ RuO₂,²⁷ V₂O₅,²⁸ and NiO²⁹ have been extensively explored as pseudocapacitive materials and shown good charge storage/energy generation performances. However, redox-active electrode materials produced from such transition MOx generally suffer from conductivity problem, poor electron transfer ability, limited surface area, high cost and toxicity.³⁰ Comparingly, π -conjugated conducting polymers offer considerable advantages such as excellent electronic conductivity, high redox capacitance, better mechanical flexibility, environmentally friendly materials, and ease of structural modification in addition to their fast switching ability between redox states during doping/dedoping process.^{31–33} Moreover, many conducting polymer derivatives can be electrochemically grown on current collector substrates without the use of any polymeric binder.

A variety of conducting polymer derivatives including polyanilines (PANI), polypyrroles (PPy), polythiophenes (PTh), poly(carbazole)s, poly(3,4-ethylenedioxythiophene) (PEDOT) have been extensively employed as redox-active electrode materials in supercapacitors.^{34–42} These conducting polymer derivatives have shown specific capacitance values in the range of 33.4–640 F g⁻¹ in different supercapacitor cell configurations. Among all polymeric pseudocapacitive materials, PEDOT and its derivatives have attracted tremendous attention owing to their fast charge/discharge rate in a relatively wider working potential window, high chemical and electrochemical stability, and suitable surface morphology although they generally have low specific capacitances. Furthermore, PEDOT can serve as both *p*-type (anode material) and *n*-type (cathode material) pseudocapacitive material for symmetric and asymmetric supercapacitor applications.^{43–46} Recently, Ermis et al. have introduced novel poly(*N*-alkylthieno[3,4-*b*][1,4]oxazine) derivatives as alternatives to PEDOT and evaluated their pseudocapacitive performances. These materials delivered better specific capacitances ($C_{\text{spec}} = 313$ and 325 F g⁻¹) and energy densities ($E = 65.24$ and 86.74 W h kg⁻¹) than those of PEDOT in organic supporting electrolyte with symmetric cell configurations.⁴⁷ However, the common disadvantage for many conducting polymer-based electrode materials is poor long-term cycling stability caused by swelling and shrinkage of the conducting polymer backbone during the Faradaic charge/discharge processes.⁴³ The design and synthesis of novel π -conjugated conducting polymers can be considered as an effective method to boost cycling stability of pseudocapacitive materials. Very recently, we have reported, for example, reasonable polymer design strategy to improve mechanical properties of redox-active materials.³⁷ The *N*-substituted poly(3,6-dithienylcarbazole) derivatives have exhibited excellent cycling performances with close to 93% capacitance retentions after 10,000 successive charge/discharge cycles owing to the high mechanical strength and flexibility of carbazole units on conducting

polymer backbone. Furthermore, poly(3,6-dithienylcarbazole)-based redox-active materials have delivered high specific capacitances ($C_{\text{spec}} = 554$ and 640 F g⁻¹) with a broad potential window of 2.0 V in flexible solid-state symmetric supercapacitor devices based on organic gel electrolyte. Our results have endorsed that molecular design approach is simple and effective tool to prepare pseudocapacitive polymeric materials with high long-term stability as well as high specific capacitance, energy, and power density.

Herein, we report syntheses and evaluation of pseudocapacitive performances of novel poly(3',4'-bis(alkyloxy)terthiophene) derivatives, poly(3',4'-dibutoxy-2,2':5',2''-terthiophene) (PTTOBu), poly(3',4'-bis(hexyloxy)-2,2':5',2''-terthiophene) (PTTOHex), and poly(3',4'-bis(octyloxy)-2,2':5',2''-terthiophene) (PTTOOct). A series of three terthiophene-based monomers were derivatized with homologous alkyl pendant groups such as butyl-, hexyl-, and octyl- and the effect of alkyl chain length on the surface morphology of polymeric redox-active network was investigated in detail. It was aimed to influence the morphological properties of pseudocapacitive layer by altering pendant groups on conducting polymer backbones and this was expected to enhance charge storage capacity of electrode material by creating suitable and efficient diffusion pathways. PTTOBu, PTTOHex, and PTTOOct-based redox-active electrodes were electrochemically prepared with minimum pseudocapacitive material mass loading on stainless steel (SS) substrates by using binder-free direct deposition method and characterized by cyclic voltammetry (CV) and galvanostatic charge/discharge (GCD) technique under a standard three-electrode cell system in organic supporting electrolyte solution. Moreover, poly(3',4'-bis(alkyloxy)terthiophene) coated SS substrates were employed as both anode and cathode materials and p-p type solid-state micro-supercapacitor devices were assembled in symmetrical two-electrode configuration. Supercapacitive performances of prototype micro-devices were tested using CV and GCD measurements with a working potential of 1.6 V. Electrochemical impedance spectroscopy (EIS) tests were further conducted to determine other electronic parameters of solid-state supercapacitor devices such as charge transfer kinetics, ion diffusion rate, and equivalent series resistance (ESR).

EXPERIMENTAL

Materials and Instrumentation

All chemicals were purchased from Sigma-Aldrich. SS substrates (99.9%, SS, 10 mm width, 10 mm length, and 0.4 mm thickness) were obtained from a local manufacturer. Before electrodeposition of conducting polymer films, SS substrates were immersed in a 2.5 M HCl solution for 5–6 min to clean potential oxide layer on the surfaces and rinsed with methanol in an ultrasonic bath and directly used. Acetonitrile (ACN) was refluxed in the presence of P₂O₅ for 8 h and fractionally distilled. ACN was stored in a brown glass bottle over activated 4A molecular sieves under a nitrogen atmosphere. Tetrabutylammonium tetrafluoroborate (Bu₄NBF₄) was dried at 85 °C for 12 h prior to use in electrochemical

studies. Fc/Fc⁺ ferrocene redox couple was used for calibration of the Ag/Ag⁺ pseudoreference silver wire (0.3 V vs. silver wire). The novel terthiophene derivatives (TTOBu, TTOHex, and TTOOct) were characterized by FTIR, NMR, mass spectroscopy, and elemental analysis techniques. The chemical structures of conducting polymer films (PTTOBu, PTTOHex, and PTTOOct) were confirmed using FTIR and elemental analysis while their morphological properties were studied with scanning electron microscopy (SEM). Conductivity measurements for PTTOBu, PTTOHex, and PTTOOct coated substrates were performed with a standard four-probe system at room temperature. A CEM Discover S-Class single-mode microwave instrument was used for nucleophilic substitution reactions. FTIR spectra were recorded with a Perkin-Elmer Spectrum 100 spectrometer (ATR apparatus). ¹H NMR and ¹³C NMR spectra were recorded on a Varian-Mercury 400 MHz (FT)-NMR spectrometer at 25 °C using tetramethylsilane internal standard. Chemical shifts were reported as ppm (δ). Mass spectra were collected on a Water 2695 Alliance Micromass ZQ LC/MS using a direct inlet probe. The morphological structures of polymeric films were observed by a Zeiss Ultra Plus FE-SEM and Zeiss EVO 40 500 V to 30 kV. Electrochemical studies were performed using a Princeton Applied Research PAR-2273 potentiostat/galvanostat and a Radiometer VoltaLab PST050 potentiostat/galvanostat-high voltage booster 100 HVB100.

Syntheses of Monomers

A multi-step reaction pathway was applied for the syntheses of novel electroactive terthiophene derivatives, 3',4'-dibutoxy-2,2':5',2''-terthiophene (TTOBu), 3',4'-bis(hexyloxy)-2,2':5',2''-terthiophene (TTOHex) and 3',4'-bis(octyloxy)-2,2':5',2''-terthiophene (TTOOct). The details of synthetic procedures and spectral data can be seen in the Supporting Information document.

Electrochemical Properties of Monomers and Their Conducting Polymers

The electrochemical redox behaviors of the novel terthiophene monomers, TTOBu, TTOHex, and TTOOct were examined by CV. CV studies were performed with a standard three-electrode cell configuration consisting of platinum wire working and auxiliary electrodes versus a Ag/Ag⁺ pseudoreference silver wire electrode. Cyclic voltammograms were recorded by scanning the potential between 0.0 and 2.0 V at 150 mV s⁻¹ scan rate in 0.1 M Bu₄NBF₄/ACN supporting electrolyte solution under a nitrogen atmosphere. Single scan CV technique was employed to evaluate p- and n-type doping properties of PTTOBu, PTTOHex, and PTTOOct polymeric films. PTTOBu, PTTOHex, and PTTOOct coated platinum wires were used as working electrodes in single scan voltammetry studies. The cyclic voltammograms of PTTOBu, PTTOHex, and PTTOOct were recorded by scanning potential between 0.0 and 2.0 V for anodic sweep and 0.0 and -2.5 V for cathodic sweep versus a Ag/Ag⁺ pseudoreference silver wire electrode in the monomer-free solution at a scan rate of 150 mV s⁻¹.

Preparation of PTTOBu, PTTOHex, and PTTOOct Redox-Active Electrode Materials

PTTOBu, PTTOHex, and PTTOOct were directly coated on the SS substrates by a constant potential electrolysis technique at suitable monomer oxidation potential (1.76 V for TTOBu, 1.79 V for TTOHex and 1.82 V for TTOOct) to control the mass loading on the SS current collectors. The constant potential electrolysis studies were performed using a SS working electrode, a SS auxiliary electrode and a Ag/Ag⁺ pseudoreference silver wire electrode with a charge density of 200 mC cm⁻² in the presence of 0.04 M monomer in 0.1 M Bu₄NBF₄/ACN supporting electrolyte solution under a nitrogen atmosphere. After deposition, PTTOBu, PTTOHex, and PTTOOct coated SS electrodes were reduced under -0.40 V constant potential for 100 s to expel trapped charges and dopant ions on the polymer surfaces. The polymeric redox-active electrodes were rinsed with ACN to remove unreacted monomer residues and ions of electrolyte. Then, the modified electrode materials were put in an oven at 70 °C for 3 h. The electroactive material mass on each SS substrate was measured six times in a row using a microanalytical balance ($\Delta m = \pm 0.001$ mg). The average of six measurements was used as total mass of redox-active material for the calculation of specific capacitance, energy density, and power density. The average mass loading of PTTOBu, PTTOHex, and PTTOOct electrodes was ~ 0.97 mg cm⁻². The chemical characterization of polymeric materials were performed by FTIR and elemental analysis techniques while the morphological properties of PTTOBu, PTTOHex, and PTTOOct coated SS substrates were probed with SEM.

Poly(3',4'-dibutoxy-2,2':5',2''-terthiophene) (PTTOBu)

IR (ATR): $\nu = 3109$ (w, aromatic C—H stretching), 2964, 2943, 2860 (w, aliphatic C—H stretching), 1634 (s, polyconjugation), 1562 (m, aromatic C=C stretching), 1458, 1375 (m, aliphatic C—H bending), 1224, 1154 cm⁻¹ (s, C—O—C stretching). Anal. calcd. for (C₂₀H₂₃O₂S₃)_n: C 61.34, H 5.92; found: C 60.97, H 6.11.

Poly(3',4'-bis(hexyloxy)-2,2':5',2''-terthiophene) (PTTOHex)

IR (ATR): $\nu = 3096$ (w, aromatic C—H stretching), 2932, 2853 (w, aliphatic C—H stretching), 1626 (s, polyconjugation), 1465, 1412, 1372 (m, aliphatic C—H bending), 1276, 1220 cm⁻¹ (s, C—O—C stretching). Anal. calcd. for (C₂₄H₃₁O₂S₃)_n: C 61.39, H 6.98; found: C 61.57, H 6.64.

Poly(3',4'-bis(octyloxy)-2,2':5',2''-terthiophene) (PTTOOct)

IR (ATR): $\nu = 3084$ (w, aromatic C—H stretching), 2938, 2864 (w, aliphatic C—H stretching), 1624 (s, polyconjugation), 1456, 1404, 1368 (m, aliphatic C—H bending), 1269, 1227 cm⁻¹ (s, C—O—C stretching). Anal. calcd. for (C₂₈H₃₉O₂S₃)_n: C 66.75, H 7.80; found: C 66.38, H 7.96.

Assembly of the Symmetric Solid-State Micro-Supercapacitor Devices

Three symmetric micro-supercapacitors were constructed by sandwiching two PTTOBu, PTTOHex, and PTTOOct redox-

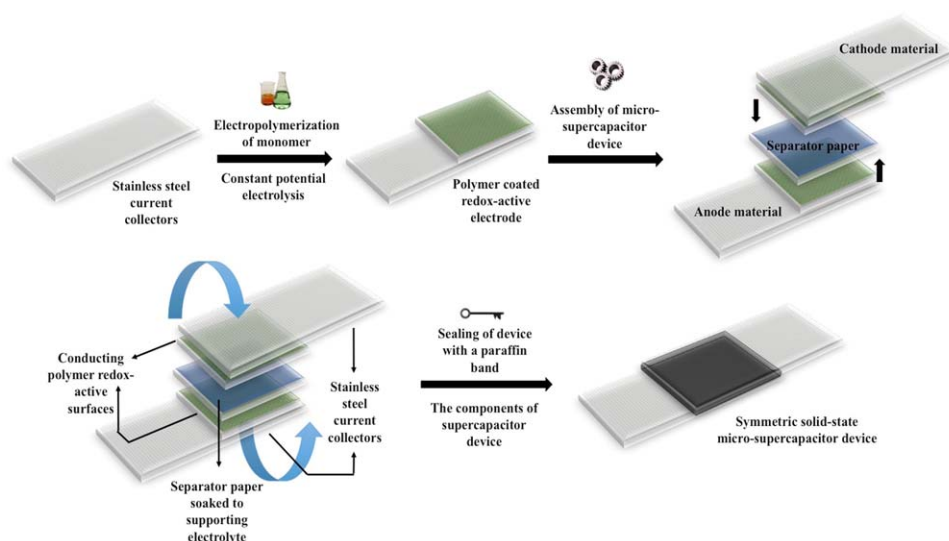


FIGURE 1 Fabrication procedure of prototype symmetric solid-state micro-supercapacitor device. [Color figure can be viewed at wileyonlinelibrary.com]

active electrodes, which were used both as anode and cathode materials in device configurations. First of all, to assemble solid-state supercapacitor devices, PTTOBu, PTTOHex, and PTTOOct electrode materials were immersed in 0.5 M $\text{Bu}_4\text{NBF}_4/\text{ACN}$ supporting solution and kept for 1 h. Thin separator paper (Whatman Grade 1 filter paper, 15 mm diameter) soaked to 0.5 M $\text{Bu}_4\text{NBF}_4/\text{ACN}$ solution was carefully placed on the polymer coated surface of one modified electrode. Then, the second redox-active electrode material was overlapped and constructed by sandwiching. In the last stage of fabrication process, the solid-state micro-supercapacitor was hermetically sealed by wrapping with a thin paraffin band. The symmetric supercapacitor devices assembled with PTTOBu, PTTOHex, and PTTOOct polymeric redox-active materials were symbolized as Device I, Device II, and Device III, respectively. Figure 1 represents a schematic diagram for preparation procedure of symmetrical solid-state micro-supercapacitor devices with a sandwich structure.

Pseudocapacitive Performance Measurements

The capacitive properties of PTTOBu, PTTOHex, and PTTOOct electrode materials were investigated by CV, GCD, and EIS techniques in both three-electrode and two-electrode cell configurations. The three-electrode measurements were carried out using polymer coated SS working and auxiliary electrodes and a Ag/Ag^+ pseudoreference silver wire electrode in 0.5 M $\text{Bu}_4\text{NBF}_4/\text{ACN}$ solution under ambient conditions. However, the capacitive performances of Device I, Device II, and Device III were tested by connecting the lead of reference electrode on the side of the auxiliary electrode. The current-potential (I - V) profiles were evaluated with CV studies in the potential range of 0.0–1.6 V at various scan rates (10, 25, 50, 100, 150, and 250 mV s^{-1}). GCD performance measurements were performed at constant current densities of 2.5, 4.5, 6.5, 8.5, 10.5, and 12.5 mA cm^{-2} in 0.0 and 1.6 V potential window. The long-term cycling stabilities

of micro-supercapacitor devices were tested by recording typical GCD curves at 2.5 mA cm^{-2} constant current density between 0.0 and 1.6 V over 10,000 charge/discharge cycles. EIS measurements were carried out with a frequency range from 10^4 to 10^{-2} Hz and voltage amplitude of 5 mV rms at 0.0 V DC voltage.

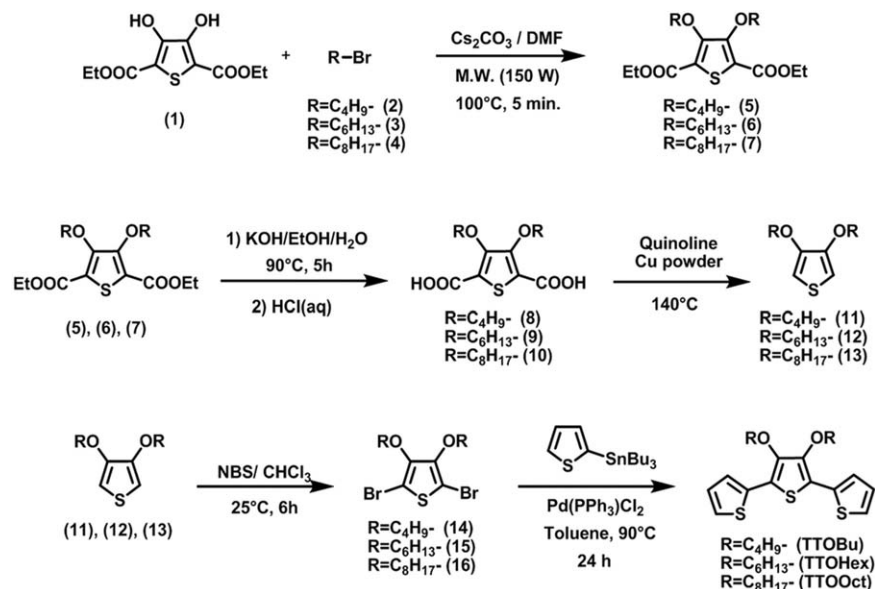
RESULTS AND DISCUSSION

Monomer Synthesis

In this study, we focused on the design, synthesis, and investigation of charge storage properties of novel terthiophene-based conducting polymers as effective redox-active materials. For this purpose, a new class of 2,2':5',2''-terthiophene monomers containing butyl-, hexyl-, and octyl- chains were initially synthesized according to a multistep synthetic procedure, as briefly illustrated in Scheme 1. The first step of synthetic pathway involves microwave-assisted nucleophilic substitution reactions of diethyl 3,4-dihydroxythiophene-2,5-dicarboxylate (**1**) with alkyl bromide compounds (**2,3,4**). Then, hydrolysis, decarboxylation and dibromination of these 3,4-bis(alkoxy)thiophenes (**5,6,7**) gave their 2,5-dibromothiophene derivatives (**14,15,16**) in good yields. The Stille cross-coupling reactions of the brominated thiophene compounds with 2-(tributylstannyl)thiophene were finally performed in the presence of $\text{Pd}(\text{PPh}_3)\text{Cl}_2$ catalyst to obtain target desired monomers, 3',4'-dibutoxy-2,2':5',2''-terthiophene (TTOBu), 3',4'-bis(hexyloxy)-2,2':5',2''-terthiophene (TTOHex), and 3',4'-bis(octyloxy)-2,2':5',2''-terthiophene (TTOOct; Fig. 2). The chemical structures of novel terthiophene monomers were confirmed by FTIR, ^1H NMR, ^{13}C NMR, mass spectroscopy, and elemental analysis techniques.

Electrochemical Characterization of Monomers and Preparation of Redox-Active Electrode Materials

TTOBu, TTOHex, and TTOOct monomers were initially subjected to CV to explore the electrochemical properties and



SCHEME 1 Synthetic pathway for **TTOBu**, **TTOHex**, and **TTOOct**.

the effect of alkyl chain lengths on the redox behaviors of novel terthiophene monomers. Voltammograms were recorded using a standard three-electrode cell configuration consisting of platinum working and auxiliary electrodes and a Ag/Ag^+ pseudoreference silver wire electrode in the potential range of 0.0 and 2.0 V at a scan rate of 150 mV s^{-1} . As can be seen from Figure 3(a–c), **TTOBu**, **TTOHex**, and **TTOOct** exhibited irreversible monomer oxidation peaks at 1.76, 1.79, and 1.82 V, respectively, in the first cycle of voltammograms. After observing monomer oxidations, characteristic reversible redox waves were appeared for **PTTOBu**, **PTTOHex**, and **PTTOOct** with an increasing current density of each successive oxidation/reduction cycle and conducting polymer films were regularly electrodeposited on the platinum surfaces. CV studies clearly reveal that **TTOOct** electroactive monomer got oxidized at slightly higher potential when compared with **TTOBu** and **TTOHex**. The small difference between oxidation potentials can be explained by the monomer solubility and steric hindrance of alkyl chains. **TTOOct** is better soluble molecule than **TTOBu** and **TTOHex** because of relatively longer alkyl chains. The increase in solubility of the monomer decreases the mobility of side alkyl chains and molecule becomes more ordered due to intense van der

Waals interaction between the alkyl chains. This effect gives the monomer a more planar structure. Thus, monomer is able to approach each other and electrode surface at a certain plane.^{48–51} Because of these reason, **TTOBu** and **TTOHex** were relatively easily oxidized than **TTOOct**.

To investigate the p- and n-doping characteristics of polymer films, single scan voltammograms were also recorded for **PTTOBu**, **PTTOHex**, and **PTTOOct** in a monomer free solution as applied in the CV procedure for monomers. Figure 3(d–f) show that all conducting polymers exhibited only p-doping property with reversible redox couples at 1.29/1.18 V for **PTTOBu**, at 1.54/0.85 V for **PTTOHex** and at 1.38/1.19 V for **PTTOOct** versus Ag wire pseudoreference electrode. The cathodic sweeps of CV curves for **PTTOBu**, **PTTOHex**, and **PTTOOct** can be seen in Fig. S1 (see Supporting Information).

After electrochemical redox characterization of all electroactive monomers (**TTOBu**, **TTOHex**, and **TTOOct**) and their corresponding polymers, conducting polymer film coated SS electrode materials were electrochemically prepared via potentiostatic method at a suitable constant potential (1.76 V for **TTOBu**, 1.79 V for **TTOHex**, and 1.82 V for **TTOOct**). **PTTOBu**, **PTTOHex**, and **PTTOOct** polymer films deposited on SS substrates were characterized by FTIR and elemental analysis techniques and found to be satisfactory. The standard four-probe technique was employed to the electrical conductivities of **PTTOBu**, **PTTOHex**, and **PTTOOct** electroactive layers. The conductivities of **PTTOBu**, **PTTOHex**, and **PTTOOct** homopolymer samples with convenient thick films ($\sim 50 \mu\text{m}$) on SS substrates were measured to be 1.7, 2.6, and 3.5 S cm^{-1} , respectively, (doped with BF_4^-) at room temperature. However, the morphological observations of conducting polymer films were performed by SEM. The top-view SEM images shown in Figure 4 confirm the homogeneous

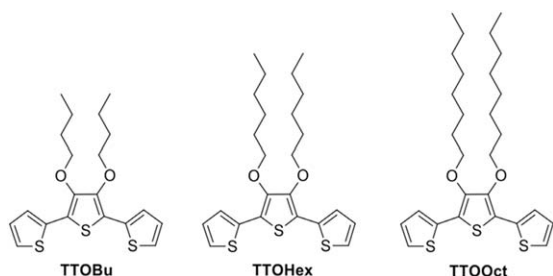


FIGURE 2 Chemical structures of the novel terthiophene monomers, **TTOBu**, **TTOHex**, and **TTOOct**.

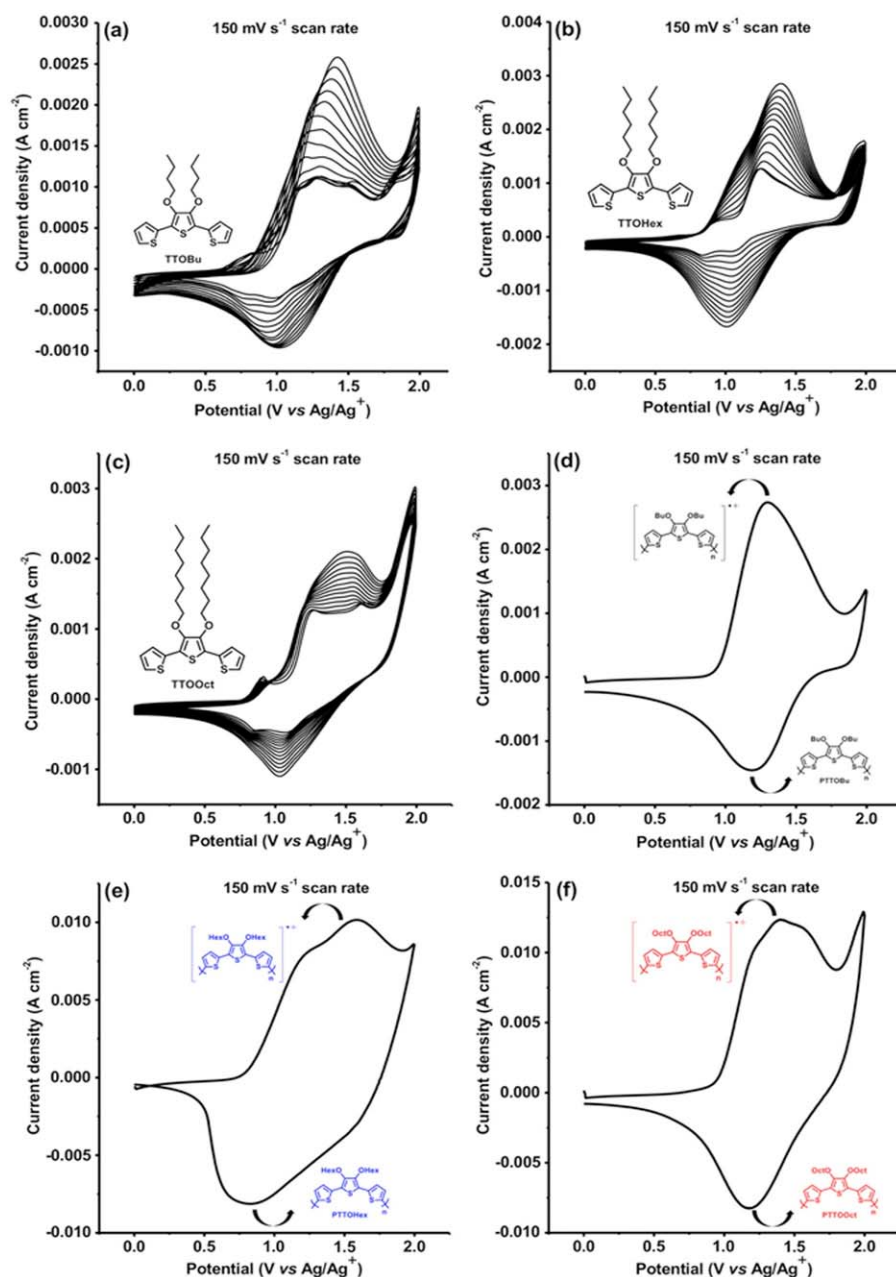


FIGURE 3 Repetitive cyclic voltammograms of (a) TTOBu, (b) TTOHex, and (c) TTOOct and single scan cyclic voltammograms of (d) PTTObu, (e) PTTOHex, and (f) PTTTOOct in a monomer free 0.1 M $\text{Bu}_4\text{NBF}_4/\text{ACN}$ solution. [Color figure can be viewed at wileyonlinelibrary.com]

formation of PTTObu, PTTOHex, and PTTTOOct polymer layer across the SS substrate surfaces. Before electropolymerization, the bare SS substrate has an ordered surface morphology [Fig. 4(a)], but after electrodeposition, Figure 4(b–k) indicate that each SS substrate was regularly coated with PTTObu, PTTOHex, and PTTTOOct.

The effect of alkyl chain on the surface morphologies of conducting polymer films can also be seen from these SEM images [Fig. 4(b,e,h)]. Prolongation of alkyl chains provides a more regular surface morphology to PTTTOOct-based conducting polymer film. As the alkyl chain length increases, the

mobility of substituents decreases due to high van der Waal interaction between alkyl groups caused by better solubility and hydrophobicity. This effect allows more regular and longer growth of polymer chains on substrate surfaces during electropolymerization process. However, as can be seen from Figure 4(b–d), conducting polymer films having shorter alkyl chains exhibit irregular surface morphologies because of self-aggregation. The regular morphological property of PTTTOOct is possible to create more effective ion diffusion pathways and enhance charge storage capability of redox-active electrode material. Conversely, the agglomerated

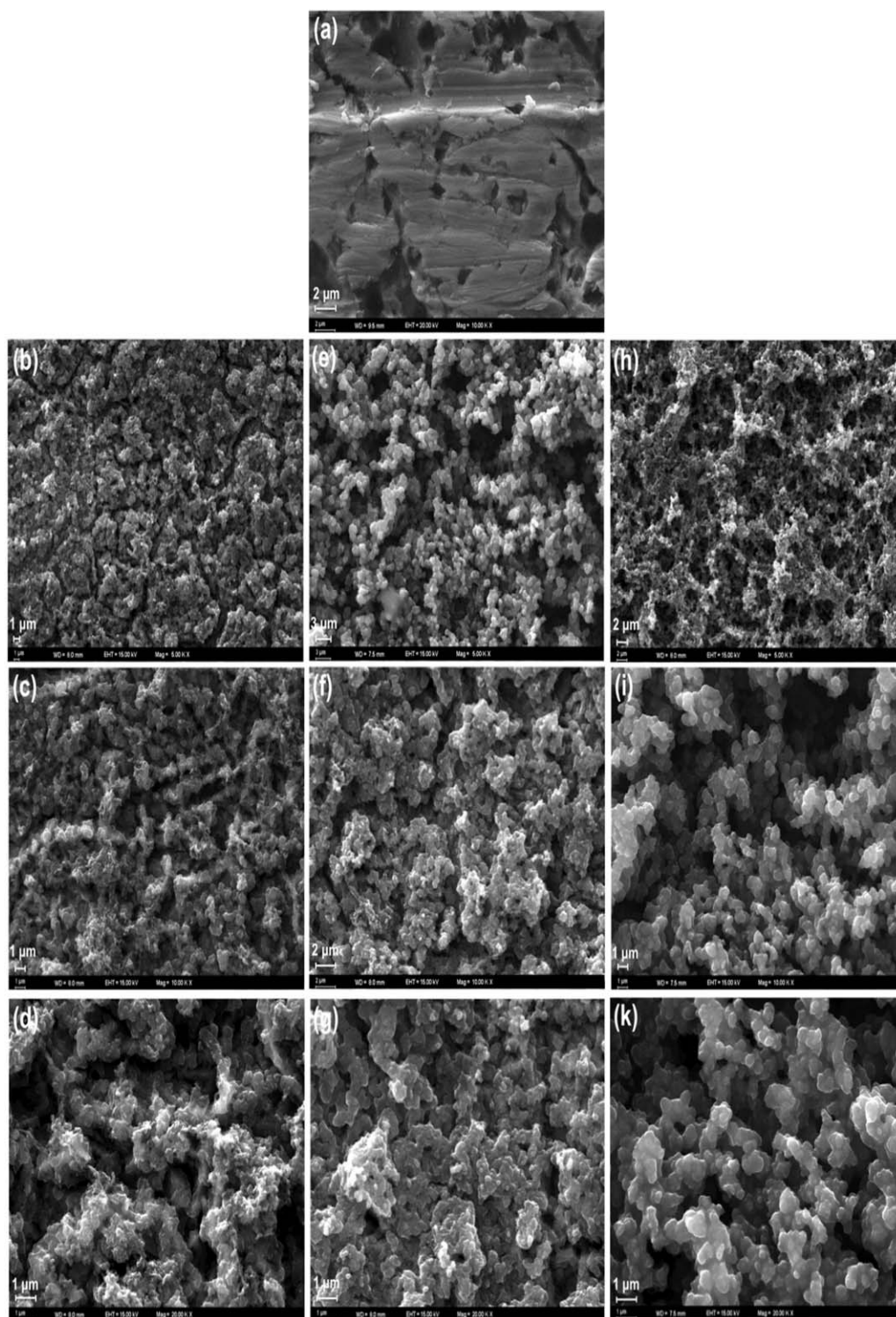


FIGURE 4 Top-view SEM images with various magnificants of (a) bare SS substrate, (b–d) PTTObu coated SS electrode materials, (e–g) PTTOHx coated SS electrode materials, and (h–k) PTTOOct coated SS electrode materials.

surface morphology of PTTObu may cause a barrier effect for ion movements. SEM observations endorse that the alkyl chain difference on conducting polymer backbone created a significant change over the surface morphologies, as expected.

Electrochemical Performance Measurements of the Redox-Active Electrode Materials

The capacitive behaviors of PTTObu, PTTOHx, and PTTOOct redox-active electrode materials were investigated by means of CV, GCD, and EIS techniques. The electrochemical

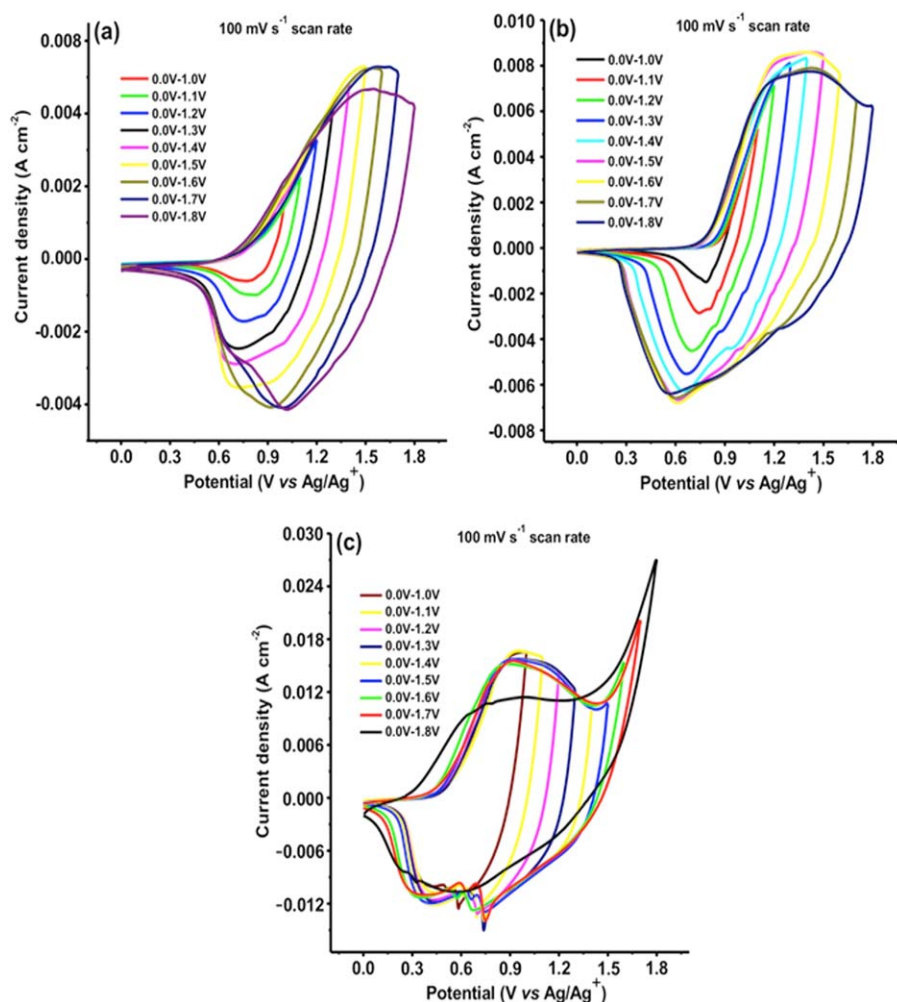


FIGURE 5 Cyclic voltammograms of (a) PTTOBu, (b) PTTOHex, and (c) PTTOOct-based polymeric redox-active materials as positive electrode in different potential windows. [Color figure can be viewed at wileyonlinelibrary.com]

measurements were performed both in a typical three-electrode cell configuration and a real supercapacitor device in two-electrode system with conducting polymer coated SS anode and cathode materials. Prior to supercapacitor performance test, the ideal working potential window was determined by preliminary CV studies for each redox-active electrode material in a symmetric three-electrode cell configuration. Figure 5(a–c) show the CV curves of PTTOBu, PTTOHex, and PTTOOct in various potential windows (range from 0.0 to 1.8 V) at 100 mV s^{-1} constant scan rate in $0.5 \text{ M Bu}_4\text{NBF}_4/\text{ACN}$ organic supporting electrolyte. Especially, it can be seen from Figure 5(b), the CV current of PTTOHex redox-active electrode material began to decrease after 1.6 V. Therefore, the potential range between 0.0 and 1.6 V was determined as optimal voltage scale for all redox-active electrode materials so as to make an objective capacitive performance comparison.

CV studies were initially carried out in 0.0 and 1.6 V potential range in order to evaluate current-potential (I–V) responses and charge/discharge characteristics of PTTOBu, PTTOHex, and PTTOOct polymeric films as redox electrode

materials. As shown Figure 6(a–c), PTTOBu, PTTOHex, and PTTOOct-based electrodes exhibited deviations from a typical rectangular-like shape in their I–V profiles due to Faradaic redox reactions as well as a pure capacitive electrical double layer. Relative to PTTOBu and PTTOHex redox-active materials, PTTOOct possess the larger normalized CV area and higher redox current density. This indicates that PTTOOct electrode material displayed better pseudocapacitive behavior than PTTOBu and PTTOHex. To investigate the effect of scan rate on CV profiles of redox materials, the cyclic voltammograms for PTTOBu, PTTOHex, and PTTOOct electrodes were also recorded at different scan rates ranging from 10 to 250 mV s^{-1} . Figure 6(a–c) display PTTOBu, PTTOHex, and PTTOOct redox-active layers still kept their I–V profiles compared to their initial shapes and the capacitive current densities increased as the sweep rate gradually increased. In addition, the oxidation/reduction redox couples for PTTOBu, PTTOHex, and PTTOOct were clearly observed even at high scan rates. These characteristic CV responses mean that our polymeric redox-active materials demonstrated high-rate reversible redox capabilities and electronic

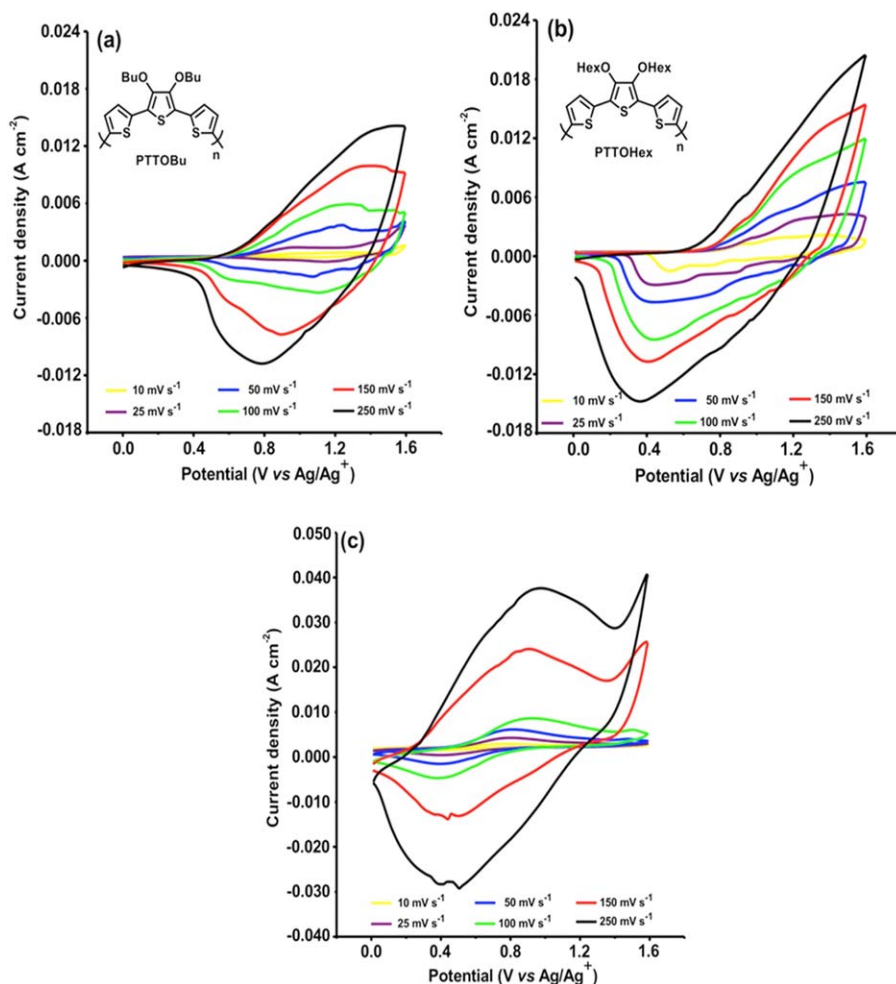


FIGURE 6 Cyclic voltammograms of (a) PTTObu, (b) PTTOHex, and (c) PTTOOct redox-active electrode materials at various scan rates (from 10 to 250 mV s^{-1}) in three-electrode cell configurations. [Color figure can be viewed at wileyonlinelibrary.com]

transportation abilities on the interface between conducting polymer surface and electrolyte during the Faradaic charge/discharge processes. The CV studies prove PTTObu, PTTOHex, and PTTOOct electrodes have good electrochemical properties and excellent redox behaviors.

Further examination of the supercapacitive performances of PTTObu, PTTOHex, and PTTOOct electrode were investigated by GCD measurements performed in a potential window of 1.6 V. It can be clearly seen from Figure 7(a-c) that polymeric redox-active electrodes exhibited linear and nearly symmetric GCD profiles with negligible ohmic drop (IR-drop) values at 2.5 mA cm^{-2} constant current density. These characteristic triangular GCD shapes reveal an excellent capacitive behavior and highly reversible Faradaic redox property as well as good balanced charge storage ability.

The specific capacitances (C_{spec} , F g^{-1}) of PTTObu, PTTOHex, and PTTOOct-based electrodes in a three-electrode configuration were calculated using the GCD curves according to eq 1:

$$C_{\text{spec}} = (I \times t_d) / (\Delta V \times m_{\text{ac}}) \quad (1)$$

where I is the discharge current (mA), t_d is the discharge time (s), ΔV is the potential change during the charge/discharge process ($V_{\text{max}} - \text{IR drop}$) (V), and m_{ac} is the mass of redox-active material in a single working electrode (mg).

The GCD measurements show the PTTOOct coated electrode material (443 F g^{-1}) delivered greatly higher specific capacitance than PTTObu (94.3 F g^{-1}) and PTTOHex (227.3 F g^{-1}) electrodes at a current density of 2.5 mA cm^{-2} . Obviously, PTTOOct redox-active layer was able to remarkably enhance its charge storage capacity owing to its more suitable polymeric network for ion movements. As expected, this morphological property most likely promoted more charge storage by facilitating faster ion diffusion during Faradaic redox processes. However, Faradaic redox reactions (doping/dedoping mechanism) occurred on PTTObu polymer chains were more limited compared with PTTOHex and PTTOOct polymeric films since the barrier effect caused by self-aggregation. This effect restricted ion diffusions required for the storage of electric charges. Thus, PTTObu redox-active electrode material has less storage capacity than PTTOHex and PTTOOct. On the basis of specific capacitance values of PTTObu,

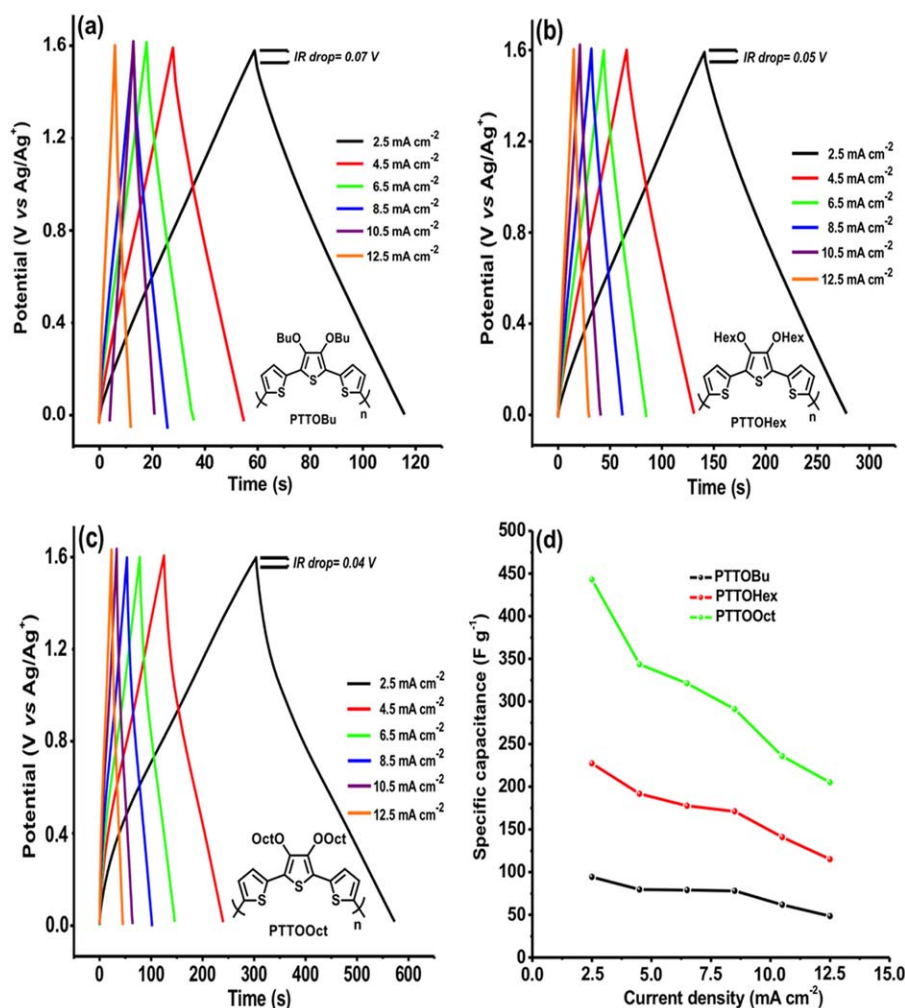


FIGURE 7 Typical GCD curves of (a) PTTOBu, (b) PTTOHex, (c) PTTOOct redox-active electrode materials at different current densities in a three-electrode cell configuration, and (d) specific capacitance values of PTTOBu, PTTOHex, and PTTOOct at various current densities. [Color figure can be viewed at wileyonlinelibrary.com]

TABLE 1 Capacitive Performances of PTh Derivatives as Redox-Active Materials

Redox-Active Material	Operating Voltage	Supporting Electrolyte	Specific Capacitance (C_{spec})	Ref
Poly(4,4'-dipentoxy-2,2':5',2''-terthiophene)	-0.27–1.03 V	1 M $\text{Et}_4\text{NBF}_4/\text{PC}$	190 F g^{-1}	17
PEDOT	-0.5–0.9 V	0.1 M NaClO_4	176 F g^{-1} at 0.75 mA cm^{-2}	39
Poly(EDOT-bithiophen-EDOT)	0.0–1.0 V	0.1 M $\text{Bu}_4\text{NPF}_6/\text{ACN}$	171 F g^{-1} at 1 A g^{-1}	40
Poly(2-(thiophene-2-yl)furan)	0.1–1.1 V	0.1 M $\text{LiClO}_4/\text{ACN}$	392 F g^{-1} at 5 A g^{-1}	41
PEDOT/PSS film	-0.8–0.8 V	0.5 M Na_2SO_4	334 F g^{-1} at 0.5 A g^{-1}	42
Poly(4-methyl-3,4-dihydro-thieno[3,4b][1,4]oxazine)	0.0–1.0 V	0.1 M $\text{Bu}_4\text{NBF}_4/\text{ACN}$	312.3 F g^{-1} at 1 mA cm^{-2}	47
Poly(4-ethyl-3,4-dihydro-thieno[3,4b][1,4]oxazine)	0.0–0.85 V	0.1 M $\text{Bu}_4\text{NBF}_4/\text{ACN}$	325.1 F g^{-1} at 1 mA cm^{-2}	47
Poly(thiophene)	-0.6–0.8 V	1 M Na_2SO_4	103 F g^{-1} at 0.3 A g^{-1}	52
Poly(3-methylthiophene)	1.15–2.0 V	1 M $\text{Et}_4\text{NBF}_4/\text{PC}$	220 F g^{-1} at 0.3 A g^{-1}	53
Poly(3',4'-ethylenedioxy-2,2':5',2''-terthiophene)	-0.2–0.5 V	1 M H_2SO_4	71 F g^{-1} at 1.5 mA cm^{-2}	54
PTTOBu	0.0–1.6 V	0.5 M $\text{Bu}_4\text{NBF}_4/\text{CAN}$	94.3 F g^{-1} at 2.5 mA cm^{-2}	This work
PTTOHex	0.0–1.6 V	0.5 M $\text{Bu}_4\text{NBF}_4/\text{ACN}$	273.3 F g^{-1} at 2.5 mA cm^{-2}	This work
PTTOOct	0.0–1.6 V	0.5 M $\text{Bu}_4\text{NBF}_4/\text{ACN}$	443 F g^{-1} at 2.5 mA cm^{-2}	This work

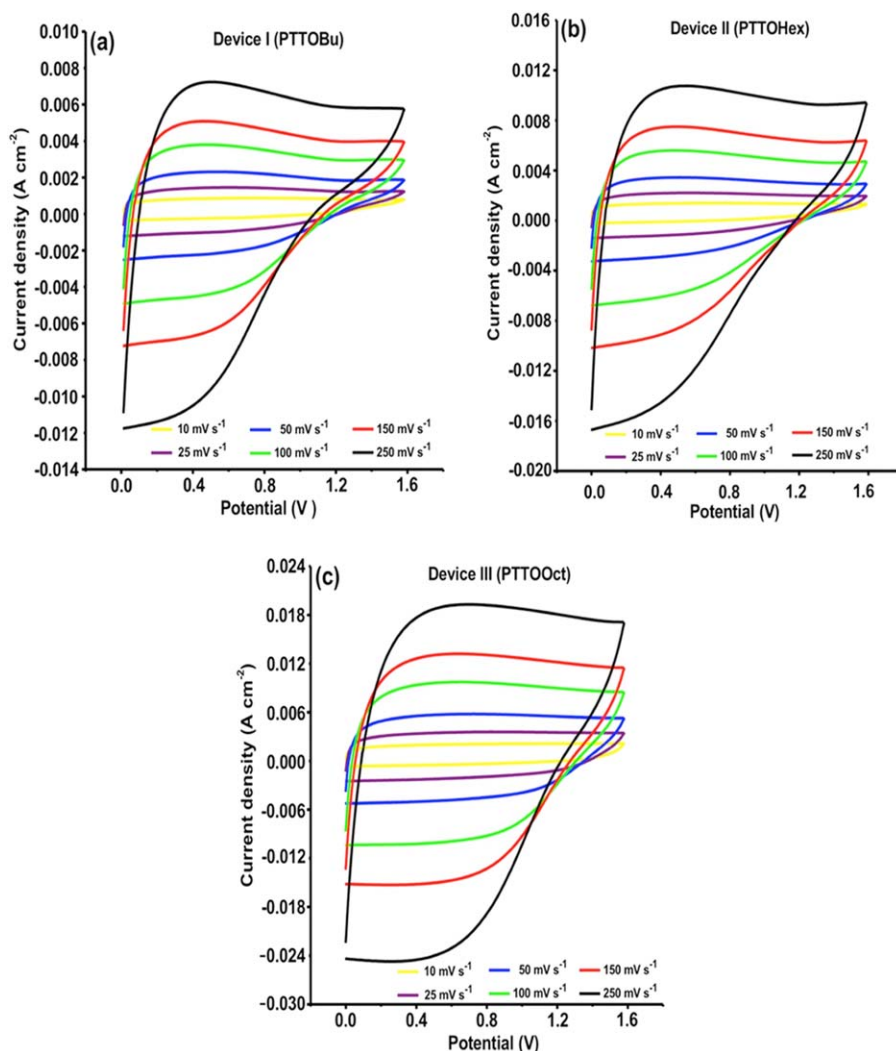


FIGURE 8 Cyclic voltammograms of (a) Device I, (b) Device II, and (c) Device III symmetric solid-state supercapacitor cells at various scan rates. [Color figure can be viewed at wileyonlinelibrary.com]

PTTOHex, and PTTOOct redox-active electrodes, it can be said that the GCD measurements are in alignment with both the CV results. The charge storage performances obtained for PTTOBu, PTTOHex, and PTTOOct-based electrodes are very competitive compared with many other poly(thiophene)-based capacitive electrode materials in the literature (Table 1).

The GCD studies were also conducted over the potential range of 0.0 to 1.6 V at various current densities from 4.5 to 12.5 mA cm⁻² to assess the rate capability performances of electrode materials. Generally, the specific capacitance of a conducting polymer-based electrode sharply decreases when the current density is increased owing to the limited ion diffusion rates and redox reactions at high discharge currents. But, as depicted in Figure 7(d), PTTOBu, PTTOHex, and PTTOOct electrode materials still managed to maintain 51.3% (from 94.3 to 48.4 F g⁻¹), 50.6% (from 227.3 to 115 F g⁻¹), and 46.3% (from 443 to 205 F g⁻¹) of their initial specific capacitance values, respectively. These rate

performances demonstrate our redox-active electrode materials exhibited good charge/discharge rate capabilities even at high current density. The high rate capability is very favorable feature in terms of fabricating electrode materials with high power density for electrochemical energy storage devices.

In addition to a three-electrode cell configuration, the capacitive performances of PTTOBu, PTTOHex, and PTTOOct electrodes were also examined by assembling p-p type symmetrical solid-state supercapacitor devices with 0.5 M Bu₄NBF₄/ACN organic supporting electrolyte. The PTTOBu, PTTOHex, and PTTOOct coated SS electrodes were employed both as anode and cathode materials for micro-supercapacitor devices in two-electrode systems. Compared with three-electrode cell configuration, the standard two-electrode setup makes it possible to obtain more realistic results, for example, the specific capacitance, energy density and power density values can be calculated for the entire supercapacitor device in all electrochemical performance

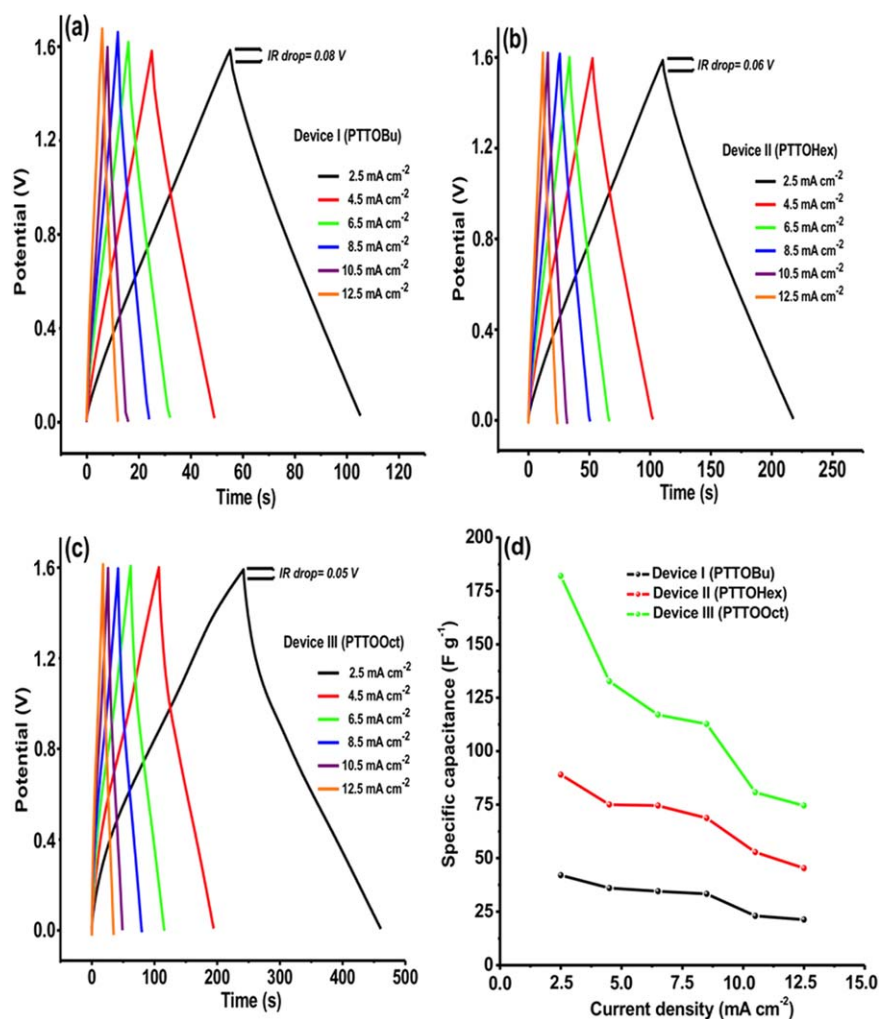


FIGURE 9 GCD curves of (a) Device I, (b) Device II, (c) Device III micro-supercapacitor cells at different current densities and (d) specific capacitance values of Device I, Device II, and Device III at various current densities. [Color figure can be viewed at wileyonlinelibrary.com]

measurements. More importantly, the supercapacitor devices with a two-electrode configuration can be easily adapted for practical electrochemical energy storage applications.

The charge storage behaviors of symmetric solid-state supercapacitor devices (Device I for PTTOBu, Device II for PTTOHex, and Device III for PTTOOct) were investigated by CV, GCD, and EIS techniques under the same conditions as in three-electrode cell measurements. Figure 8(a–c) show the CV curves of micro-supercapacitor devices at scan rates of 10, 25, 50, 100, 150, and 250 mV s⁻¹ within the applied potential range 0.0–1.6 V. As expected from a two-electrode cell configuration, Device I, Device II, and Device III exhibited I–V profiles closer to rectangular shape form compared with the CV curves in three-electrode configuration.

From Figure 8(a–c), it is clearly seen that both the CV current and area under the voltammograms of Device III are significantly higher than those of Device I and Device II, indicating better capacitive nature of PTTOOct. Moreover, no

shape changes were observed for Device I, Device II and Device III micro-supercapacitors with an increasing scan rate from 10 to 250 mV s⁻¹. These electrochemical behaviors can be directly correlated with good rate capabilities and low contact resistances of PTTOBu, PTTOHex, and PTTOOct polymeric films.

GCD curves of Device I, Device II, and Device III in the potential range between 0.0 and 1.6 V are given in Figure 9(a–c). The effect of fast ion transport kinetics and highly reversible Faradaic redox reaction behaviors of PTTOBu, PTTOHex, and PTTOOct-based electrode materials openly appeared in the GCD cycle characteristics of micro-supercapacitor devices. Device I, Device II, and Device III displayed a typical triangular GCD profiles at a constant current density of 2.5 mA cm⁻². The small ohmic drops (IR-drop) were also determined to be 0.08, 0.06, and 0.05 V for Device I, Device II, and Device III, respectively. This result confirms that PTTOBu, PTTOHex, and PTTOOct redox-active electrode materials have low internal resistances.

TABLE 2 Specific Capacitance, Energy Density, and Power Density Values of Solid-State Micro-Supercapacitor Devices

Micro-supercapacitor device	Specific capacitance (C_{spec}) F g^{-1}	Energy density (E) W h kg^{-1}	Power density (P) kW kg^{-1}
Device I	42	13.5	0.98
Device II	89	29.3	1
Device III	182	60.7	1.1

The values of specific capacitance (C_{spec} F g^{-1}), energy density (E , W h kg^{-1}), and power density (P , kW kg^{-1}) of micro-supercapacitor devices were calculated using GCD curves at 2.5 mA cm^{-2} from the following eqs (2–4):

$$C_{\text{spec}} = (I \times t_d) / (\Delta V m_{\text{ac}}) \quad (2)$$

$$E = [C_{\text{spec}} \times (\Delta V)^2] / 7.2 \quad (3)$$

$$P = (3600 \times E) / t_d \quad (4)$$

where I is the discharge current (mA), t_d is the discharge time (s), ΔV is the potential change during the discharge cycle ($V_{\text{max}} - \text{IR drop}$) (V), and m_{ac} is the total mass of redox-active material in two electrodes (mg).

As presented in Table 2, Device I, Device II, and Device III reached up to 42, 89, and 182 F g^{-1} specific capacitance

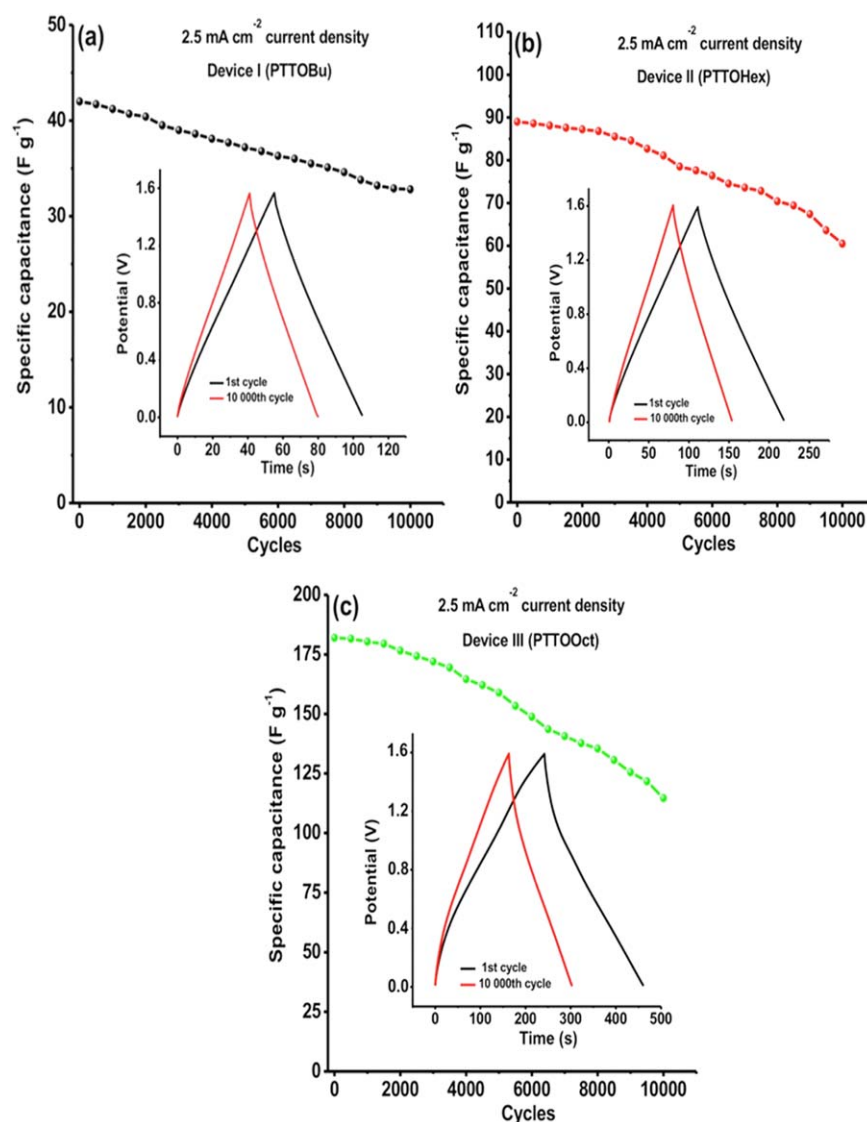


FIGURE 10 Long-term cycling stabilities of (a) Device I, (b) Device II, and (c) Device III at 2.5 mA cm^{-2} constant current density for 10,000 charge/discharge cycles. [Color figure can be viewed at wileyonlinelibrary.com]

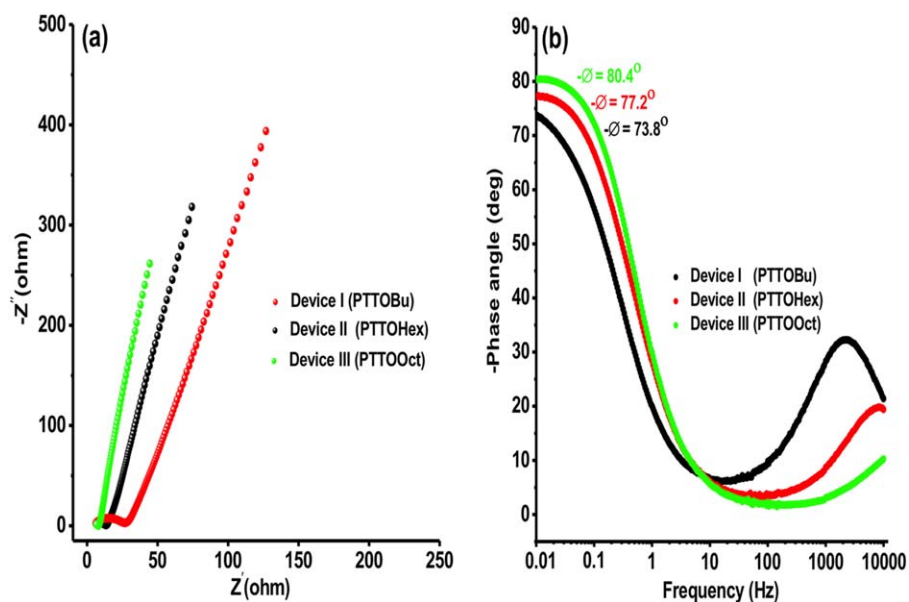


FIGURE 11 (a) Comparative Nyquist plots of supercapacitor devices with a frequency range from 10^4 to 10^{-2} Hz and voltage amplitude of 5 mV rms at 0.0 V DC voltage and (b) comparative Bode-phase angle plots of Device I, Device II, and Device III micro-supercapacitors. [Color figure can be viewed at wileyonlinelibrary.com]

values. On the other side, Device I, Device II, and Device III delivered energy densities of 13.5, 29.3, and 60.7 W h kg^{-1} and power densities of 0.98, 1, and 1.1 kW kg^{-1} , respectively. Figure 9(a–c) indicates that Device III had the longest discharging duration than Device I and Device II, which implies more suitable morphology of PTTOOct redox-active layer. The rate capabilities of micro-supercapacitor devices were explored by recording the GCD curves at various current densities of 4.5, 6.5, 8.5, 10.5, and 12.5 mA cm^{-2} . Device I, Device II, and Device III retained 50.7, 50.9, and 41% of their gravimetric capacitances, respectively, when current density was increased, as seen from Figure 9(d). The electrochemical characterization data collected for Device I, Device II, and Device III agree well with the CV and GCD results of redox-active electrodes obtained in a three-electrode cell configurations.

For practical supercapacitor applications, long-term cycling stability is another important performance parameter as well as specific capacitance, energy and power density and rate capability. The cycling stability performance of our symmetrical micro-supercapacitor devices were evaluated using a typical GCD measurement at a constant current density of 2.5 mA cm^{-2} between 0.0 and 1.6 V for 10 000 charge/discharge cycles. The variations of specific capacitances in Device I, Device II, and Device III as a function of GCD cycles are depicted in Figure 10(a–c). At the end of 10,000 cycles, Device I, Device II, and Device III exhibited 78, 68, and 63% capacitance retentions, respectively. The cycling stability tests clearly reveal that PTTOOct redox-active surface (Device III) could tolerate the volumetric surface degradation less than PTOOBu (Device I) and PTTOHex (Device II). This situation is probably due to the more Faradaic reactions occurring on PTTOOct polymeric network during long-term charge/discharge cycling.

Finally, EIS technique was employed to analyze electronic properties of Device I, Device II, and Device III such as internal resistance (ESR), charge transfer resistance (RCT), and ion diffusion kinetics and rates. EIS spectra were recorded using a perturbation amplitude of 5 mV rms with a frequency range from 10^4 to 10^{-2} Hz at an applied DC voltage of 0.0 V. As displayed in Figure 11(a), all Nyquist plots are composed of a semi-circle pattern in the high-frequency region and a straight line portion in the low-frequency region, which is characteristic impedance response for supercapacitors based on conducting polymers.

In the high-frequency region, the ESR of Device I, Device II, and Device III were determined to be 5.9, 7.1, and 6.5Ω , respectively, from the intercept point of Z'-axis and the starting point of semi-circle. ESR is described as the combined resistance involving the ionic resistance of electrolyte, the electronic resistance of the electroactive material and the contact resistance between electrode material and current collector. In this context, these low ESR values of micro-supercapacitor devices stand for PTOOBu, PTTOHex, and PTTOOct polymeric networks possess low internal resistance, indicating reasonable electronic property for solid-state practical supercapacitor applications. In addition, the charge transfer resistance (R_{CT}) values were directly obtained by the diameter of semi-circle in the high-frequency region. Figure 11(a) demonstrate that Device III has a smaller radius semi-circle pattern ($R_{CT} = 1.6 \Omega$) than those of Device I ($R_{CT} = 20 \Omega$) and Device II ($R_{CT} = 6.3 \Omega$). This means that PTTOOct polymer film was uniformly coated on the SS current collector and the interaction between PTTOOct redox-active network and SS interface was stronger compared with PTOOBu and PTTOHex polymeric structures.

In the low-frequency region, each Nyquist plot exhibited a straight line, Warburg portion, toward the Z' real axis with an increase in the imaginary part ($-Z''$ -axis). As can be seen from Figure 11(a), the Warburg regions of Device I and Device II are longer than that of Device III. This difference between impedance characteristics is thought to be a result of relatively slower ion diffusion rates and longer diffusion pathways in the polymeric networks of PTTObu and PTTOHex. The more suitable 3D-dimensional morphology of PTTOOct conducting film helped to improve ion movements in Device III by offering sufficient and shorter diffusion path lengths compared with the morphologies of PTTObu (Device I) and PTTOHex (Device II). Moreover, the Warburg region of Device III has also a steeper slope than those of Device I and Device II. This means that an electrochemical double-layer was formed faster on PTTOOct surface and it had a better capacitive performance under the same condition. In addition to Nyquist plots, the Bode-phase angle plots were also recorded in the frequency range of 10^4 to 10^{-2} Hz [Fig. 11(b)]. In the Bode plots, the phase angles of Device I, Device II, and Device III corresponded to -73.8° , -77.2° , and -80.4° at 10^{-2} Hz. According to Bode-phase angle analyses, it can be said that Device III has a better pseudocapacitive performance than Device I and Device II since the capacitive behavior in the low-frequency region is usually determined with the phase angle approaching -90° . These experimental data also prove that PTTObu, PTTOHex, and PTTOOct exhibit good electrochemical capacitive properties and claim potential application as redox-active electrode materials in energy storage devices.

CONCLUSIONS

In summary, we successfully prepared a series of the novel poly(terthiophene) derivatives, PTTObu, PTTOHex, and PTTOOct, specifically designed to control the morphology of polymeric network and enhance the charge storage capacity of electrode material. The SEM studies revealed that increase in the alkyl chain length of the polymer backbones created a remarkable change over the morphologies and caused suitable network for more effective ion diffusions. The electrochemical performance tests also endorsed the success of the molecular design approach used to enhance the capacitive properties of conducting polymer-based electrode materials. PTTOOct redox-active electrode material delivered higher maximum specific capacitance (443 F g^{-1}) than PTTOHex (227.3 F g^{-1}) and PTTObu (94.3 F g^{-1}) thanks to its relatively more suitable 3D-dimensional polymeric network, which allows easier and faster ion diffusion. In addition, PTTObu, PTTOHex, and PTTOOct-based electrodes reached up to 42, 89, and 182 F g^{-1} specific capacitance values, respectively, in symmetric solid-state micro-supercapacitor device configurations. Micro-supercapacitor devices exhibited satisfactory energy densities (13.5 W h kg^{-1} for Device I, 29.3 W h kg^{-1} for Device II, and 60.7 W h kg^{-1} for Device III) and power densities (0.98 kW kg^{-1} for Device I, 1 kW kg^{-1} for Device II and 1.1 kW kg^{-1} for Device III). Moreover, our symmetric supercapacitor devices achieved good capacitance

retentions upon long-term charge/discharge cycling after 10,000 cycles. In this context, the capacitive performances of PTTObu, PTTOHex, and PTTOOct were found to be comparable to various polymeric redox electrode materials such as PTh, PPy, and PANI derivatives, previously reported.^{17,39–45,47,52–57} The results reveal that molecular design strategy could be beneficial for the preparation of novel pseudocapacitive electrode materials with controllable morphology and improved performance.

ACKNOWLEDGMENTS

The authors thank the Scientific and Technological Research Council of Turkey (TÜBİTAK, Grant No: KBAG-114Z167) for financial support. D. Yiğit is also generously supported by TÜBİTAK KBAG-114Z167 with a postdoctoral scholarship. They also would like to thank Elif Akhüseyin Yıldız for her assistance with the SEM observations.

REFERENCES AND NOTES

- 1 R. Francke, D. Cericola, R. Kötz, G. Schnakenburg, S. R. Waldvogel, *Chem. Eur. J.* **2011**, *17*, 3082.
- 2 Y. Xu, J. Wang, Z. Chang, B. Ding, Y. Wang, L. Shen, C. Mi, H. Dou, X. Zhang, *Chem. Eur. J.* **2016**, *22*, 4256.
- 3 G. Xu, B. Ding, P. Nie, L. Shen, J. Wang, X. Zhang, *Chem. Eur. J.* **2013**, *19*, 12306.
- 4 T. Chen, L. Dai, *J. Mater. Chem. A* **2014**, *2*, 10756.
- 5 L. Dong, C. Xu, Y. Li, Z. Huang, F. Kang, Q. Yang, X. Zhao, *J. Mater. Chem. A* **2016**, *4*, 4659.
- 6 X. Zhang, Z. Lin, B. Chen, S. Sharma, C. Wong, W. Zhang, Y. Deng, *J. Mater. Chem. A* **2013**, *1*, 5835.
- 7 J. Liu, J. G. Zhang, Z. Yang, J. P. Lemmon, C. Imhoff, G. L. Graff, L. Li, J. Hu, C. Wang, J. Xiao, G. Xia, V. V. Viswanathan, S. Baskaran, V. Sprenkle, X. Li, Y. Shao, B. Schwenzer, *Adv. Funct. Mater.* **2013**, *23*, 929.
- 8 M. Pumera, *Chem. Eur. J.* **2009**, *15*, 4970.
- 9 T. Chen, L. Dai, *Mater. Today* **2013**, *16*, 272.
- 10 R. R. Salunkhe, Y. H. Lee, K. H. Chang, J. M. Li, P. Simon, J. Tang, N. L. Torad, C. C. Hu, Y. Yamauchi, *Chem. Eur. J.* **2014**, *20*, 13838.
- 11 J. Zhang, J. Xu, D. Zhang, *J. Electrochem. Soc.* **2016**, *163*, E83.
- 12 C. Ma, Y. Yu, Y. Li, J. Shi, Y. Song, L. Liu, *J. Electrochem. Soc.* **2014**, *161*, A1330.
- 13 S. M. Jung, D. L. Mafra, C. Lin, H. Y. Jung, J. Kong, *Nanoscale* **2015**, *7*, 4386.
- 14 A. G. Pandolfo, A. F. Hollenkamp, *J. Power Sources* **2006**, *157*, 11.
- 15 L. L. Zhang, X. S. Zhao, *Chem. Soc. Rev.* **2009**, *38*, 2520.
- 16 M. Huang, F. Li, F. Dong, Y. X. Zhang, L. L. Zhang, *J. Mater. Chem. A* **2015**, *3*, 21380.
- 17 C. Arbizzani, M. C. Gallazzi, M. Mastragostino, M. Rossi, F. Soavi, *Electrochem. Commun.* **2001**, *3*, 16.
- 18 P. Soudan, P. Lucas, H. A. Ho, D. Jobin, L. Breau, D. Belanger, *J. Mater. Chem.* **2001**, *11*, 773.
- 19 C. D. Lokhande, D. P. Dubal, O. S. Joo, *Curr. Appl. Phys.* **2011**, *11*, 255.

- 20 Y. B. He, G. R. Li, Z. L. Wang, C. Y. Su, Y. X. Tong, *Energy Environ. Sci.* **2011**, *4*, 1288.
- 21 N. L. Wu, *Mater. Chem. Phys.* **2002**, *75*, 6.
- 22 L. Fan, J. Maier, *Electrochem. Commun.* **2006**, *8*, 937.
- 23 K. R. Prasad, K. Koga, N. Miura, *Chem. Mater.* **2004**, *16*, 1845.
- 24 H. Zhou, Y. Zhang, *J. Phys. Chem. C* **2014**, *118*, 5626.
- 25 T. Brousse, M. Toupin, R. Dugas, L. Athouel, O. Crosnier, D. Belanger, *J. Electrochem. Soc.* **2006**, *153*, A2171.
- 26 Y. Liu, Y. Jiao, Z. Zhang, F. Qu, A. Umar, X. Wu, *ACS Appl. Mater. Interfaces* **2014**, *6*, 2174.
- 27 H. Xia, Y. Shirley Meng, G. Yuan, C. Cui, L. Lu, *Electrochem. Solid State Lett.* **2012**, *15*, A60.
- 28 B. Saravanakumar, K. K. Purushothaman, G. Muralidharan, *ACS Appl. Mater. Interfaces* **2012**, *4*, 4484.
- 29 C. Yuan, X. Zhang, L. Su, B. Gao, L. Shen, *J. Mater. Chem.* **2009**, *19*, 5772.
- 30 M. Zhi, C. Xiang, J. Li, M. Li, N. Wu, *Nanoscale* **2013**, *5*, 72.
- 31 G. Wang, L. Zhang, J. Zhang, *Chem. Soc. Rev.* **2012**, *41*, 797.
- 32 K. Wang, H. Wu, Y. Meng, Z. Wei, *Small* **2014**, *10*, 14.
- 33 S. M. Chen, R. Ramanchandran, V. Mani, R. Saraswathi, *Int. J. Electrochem. Sci.* **2014**, *9*, 4072.
- 34 H. Wang, J. Lin, Z. X. Shen, *Adv. Mater. Devices* **2016**, *1*, 225.
- 35 Y. Huang, H. Li, Z. Wang, M. Zhu, Z. Pei, Q. Xue, Y. Huang, C. Zhi, *Nano Energy* **2016**, *22*, 422.
- 36 T. M. S. K. Pathiranage, D. S. Dissanayake, C. N. Niermann, Y. Ren, M. C. Beiwer, M. C. Stefan, *J. Polym. Sci. Part A: Polym. Chem.* **2017**, *55*, 3327.
- 37 D. Yiğit, M. Güllü, *J. Mater. Chem. A* **2017**, *5*, 609.
- 38 D. Yiğit, M. Güllü, T. Yumak, A. Sınaç, *J. Mater. Chem. A* **2014**, *2*, 6512.
- 39 S. Patra, N. Munichandraiah, *J. Appl. Polym. Sci.* **2007**, *106*, 1160.
- 40 D. Mo, W. Zhou, X. Ma, J. Xu, D. Zhu, B. Lu, *Electrochim. Acta* **2014**, *132*, 67.
- 41 D. Mo, W. Zhou, X. Ma, J. Xu, *Electrochim. Acta* **2015**, *155*, 29.
- 42 W. Zhou, J. Xu, *Electrochim. Acta* **2016**, *222*, 1895.
- 43 K. S. Ryu, Y. G. Lee, Y. S. Hong, Y. J. Park, X. Wu, K. M. Kim, M. G. Kang, N. G. Park, S. H. Chang, *Electrochim. Acta* **2004**, *50*, 843.
- 44 C. Arbizzani, M. Mastragostino, L. Meneghello, *Electrochim. Acta* **1996**, *41*, 21.
- 45 J. H. Huang, C. W. Chu, *Electrochim. Acta* **2011**, *56*, 7228.
- 46 V. Armel, J. Rivnay, G. Malliaras, B. W. Jensen, *J. Am. Chem. Soc.* **2013**, *135*, 11309.
- 47 E. Ermiş, D. Yiğit, M. Güllü, *Electrochim. Acta* **2013**, *90*, 623.
- 48 J. Roncali, R. Garreau, A. Yassar, P. Marque, F. Garnier, M. Lemaire, *J. Phys. Chem.* **1987**, *91*, 6706.
- 49 J. Roncali, *Chem. Mater.* **1993**, *5*, 1456.
- 50 I. Namal, A. C. Ozeltaglayan, Y. A. Udum, L. Toppare, *Eur. Polym. J.* **2013**, *49*, 3181.
- 51 D. Mo, S. Zhen, J. Xu, W. Zhou, B. Lu, G. Zhang, Z. Wang, S. Zhang, Z. Feng, *Synth. Met.* **2014**, *198*, 19.
- 52 H. Zhang, L. Hu, J. Tu, S. Jiao, *Electrochim. Acta* **2014**, *120*, 122.
- 53 M. Mastragostino, C. Arbizzani, F. Soavi, *Solid State Ionics* **2002**, *148*, 493.
- 54 T. Abdiryim, R. Jamal, C. Zhao, T. Awut, I. Nurulla, *Syn. Met.* **2010**, *160*, 325.
- 55 K. S. Ryu, K. M. Kim, N. G. Park, Y. J. Park, S. H. Chang, *J. Power Sources* **2002**, *103*, 305.
- 56 R. K. Sharma, A. C. Rastogi, S. B. Desu, *Electrochem. Commun.* **2008**, *10*, 268.
- 57 D. Yiğit, T. Güngör, M. Güllü, *Org. Electron.* **2013**, *14*, 3249.